Biophysical Journal
Article

Biophysical Society

Cytoskeleton Remodeling Induces Membrane Stiffness and Stability Changes of Maturing Reticulocytes

He Li,[1,*] Jun Yang,[2] Trang T. Chu,[3,4] Renugah Naidu,[3] Lu Lu,[1] Rajesh Chandramohanadas,[3] Ming Dao,[2,4] and George Em Karniadakis[1,*]

[1]Division of Applied Mathematics, Brown University, Providence, Rhode Island; [2]Department of Materials Science and Engineering, Massachusetts Institute of Technology, Cambridge, Massachusetts; [3]Pillar of Engineering Product Development, Singapore University of Technology and Design, Singapore, Singapore; and [4]Interdisciplinary Research Group of Infectious Diseases, Singapore-MIT Alliance for Research and Technology Centre, Singapore, Singapore

ABSTRACT Reticulocytes, the precursors of erythrocytes, undergo drastic alterations in cell size, shape, and deformability during maturation. Experimental evidence suggests that young reticulocytes are stiffer and less stable than their mature counterparts; however, the underlying mechanism is yet to be fully understood. Here, we develop a coarse-grained molecular-dynamics reticulocyte membrane model to elucidate how the membrane structure of reticulocytes contributes to their particular biomechanical properties and pathogenesis in blood diseases. First, we show that the extended cytoskeleton in the reticulocyte membrane is responsible for its increased shear modulus. Subsequently, we quantify the effect of weakened cytoskeleton on the stiffness and stability of reticulocytes, via which we demonstrate that the extended cytoskeleton along with reduced cytoskeleton connectivity leads to the seeming paradox that reticulocytes are stiffer and less stable than the mature erythrocytes. Our simulation results also suggest that membrane budding and the consequent vesiculation of reticulocytes can occur independently of the endocytosis-exocytosis pathway, and thus, it may serve as an additional means of removing unwanted membrane proteins from reticulocytes. Finally, we find that membrane budding is exacerbated when the cohesion between the lipid bilayer and the cytoskeleton is compromised, which is in accord with the clinical observations that erythrocytes start shedding membrane surface at the reticulocyte stage in hereditary spherocytosis. Taken together, our results quantify the stiffness and stability change of reticulocytes during their maturation and provide, to our knowledge, new insights into the pathogenesis of hereditary spherocytosis and malaria.

INTRODUCTION

Human erythrocytes (red blood cells (RBCs)) are produced through erythropoiesis, in which hematopoietic stem cells derived in the bone marrow gradually transition to erythrocytes via a series of differentiations (1,2). In the late stage of differentiation, normoblasts expel nucleus and form stiff, multilobular reticulocytes. Young reticulocytes are confined to the bone marrow for ~24 h before their egress to circulation, where they mature to erythrocytes after an additional ~24 h (3). During maturation, reticulocytes expel unwanted membrane proteins such as transferrin receptor (CD71), CD98, and integrin $\alpha 4\beta 1$ via releasing small vesicles called exosomes (4–7). Exosome secretion contributes to the cell surface decrease and shape transition from multilobular to biconcave (8–10). In addition to the striking morphological change, the deformability and stability of reticulocytes increase as they mature (11–13). Maturing reticulocytes have been classified into different stages based on their morphology and membrane shear moduli (14). Enucleation of late-stage erythroblasts generates nascent reticulocytes, which are motile, multilobulated cells (R1 stage). As reticulocytes mature, they lose motility and transform into asymmetrical deep-dish-shaped cells with a refractile ring and visible granules (R2 stage). During the subsequent maturation, the visible granules inside the reticulocytes disappear (R3 stage). Eventually, these deep-dish-shaped cells assume a biconcave shape. The shear modulus measured from the reticulocytes at different stages of maturation shows that the value of the shear modulus decreases from 11.4 μN/m

Submitted December 14, 2017, and accepted for publication March 6, 2018.

*Correspondence: he_li@brown.edu or george_karniadakis@brown.edu

He Li, Jun Yang, and Trang T. Chu contributed equally to this work.

Editor: D. Peter Tieleman.

https://doi.org/10.1016/j.bpj.2018.03.004

(R1 stage) to 8.6 μN/m (R2 stage) and to 6.1 μN/m (R3 stage) (13). It is noted that the shear modulus of late-stage reticulocytes (R3) is similar to the shear modulus of 3.7 $\pm$ 2.3 μN/m for mature RBCs (15). Although reticulocytes at the R1 and R2 stages are stiffer than erythrocytes, they are less stable, as reticulocytes break into fragments in the micropipette and ektacytometry experiments (11). Furthermore, membrane budding and subsequent microvesiculation were observed at the late stages of reticulocyte maturation (16), confirming the previous finding on the instability of the cell membrane. More importantly, shedding cell surface proteins via membrane budding provides an alternative pathway for removing nonessential membrane integral proteins from reticulocytes and thus could be a part of the reticulocyte maturation process. Recent experimental evidence suggested that membrane budding and microvesiculation were expedited in the reticulocytes infected with *Plasmodium vivax* (17), indicating that *P. vivax* can exacerbate the membrane instability.

In contrast to the biconcave shape of mature erythrocytes, the multilobular appearance of reticulocytes undoubtedly contributes to their greater stiffness. Additionally, Chasis et al. (18) speculated that the stiffness and instability of reticulocytes may result from the structure of cell membrane. Reticulocytes possess larger surface area than that of mature erythrocytes (9,10), and thus, the cytoskeleton underneath the lipid bilayer could be under extension, leading to increased membrane stiffness. On the other hand, the instability of reticulocytes may originate from the temporal difference on the synthesis and expression of the cytoskeletal proteins. Prior studies showed that the components of the membrane cytoskeleton were assembled at different stages of maturation (11,19–23). For example, the synthesis of spectrin tetramer was already completed at the reticulocyte stage, whereas protein 4.1 and glycophorin C were still being synthesized. Protein 4.1 and glycophorin C are essential for maintaining the integrity of the erythrocyte membrane. Glycophorin C is responsible for tethering the cytoskeletal network to the lipid bilayer via additional binding proteins, such as protein 4.1 and adducin (24). Protein 4.1 consolidates the association between the spectrin tetramers and actin junctions (25,26). Hence, the absence of either protein 4.1 or glycophorin C could result in a weak cohesion between the lipid bilayer and cytoskeleton (27).

Reticulocytes only account for $\sim$1% of the erythrocyte population in blood under physiological conditions and thus play little role in gaseous exchange or nutrient transport. However, the reticulocytes can occupy more than 10% of the erythrocyte population in case of severe hemolytic anemia, such as in sickle cell anemia, hereditary spherocytosis (HS), and hereditary elliptocytosis (28,29). In addition, the particular biochemical and biomechanical properties of reticulocytes are related to the pathogenesis of several blood diseases. For example, sickle reticulocytes assume a multispiculated appearance after deoxygenation, and they are more adhesive than the mature sickle erythrocytes (30–32). Defective erythrocytes in HS tend to shed surface area at the reticulocyte stage (10). Malaria parasites *P. vivax* and *Plasmodium falciparum* both prefer young reticulocytes for infection (17,33–36), which may result not only from the presence of specific receptors on the reticulocyte membrane (37,38) but also from the particular morphology and biophysical properties of reticulocytes. Therefore, understanding the membrane structure of reticulocytes and the consequent biomechanical properties can provide new insights into the pathophysiology of blood diseases. Although reticulocyte membrane remodeling during maturation has been studied extensively (11,26,39–41), the structural change of the membrane cytoskeleton during remodeling is still not fully understood. In addition, specific protein-protein associations were examined in the immature and mature erythrocyte membrane, through which significant distinctions were discovered at the actin junction complexes (26), but the means by which these altered protein interactions lead to the stiffer but less-stable reticulocytes has yet to be dissected in detail.

In this work, we develop a coarse-grained molecular-dynamics (CGMD) reticulocyte membrane model to examine the molecular basis for the particular biomechanical properties of reticulocytes and investigate the mechanisms causing the increased stiffness but decreased stability of reticulocytes. The reticulocyte membrane model is constructed based on recent atomic force microscopy (AFM) imaging on the cytoplasmic surface of the reticulocyte membrane (15) as well as prior studies of protein expression and association in the reticulocyte membrane (26). The applied CGMD membrane model can represent the observed reticulocyte cytoskeletal structure from AFM and evaluate the corresponding shear modulus. The computed shear moduli are validated and compared with the micropipette measurements of immature reticulocytes and mature RBCs. Then, we use the validated reticulocyte membrane model to study the instability of the reticulocytes and explore how the membrane instability contributes to the vesiculation of reticulocytes in HS.

MATERIALS AND METHODS

Micropipette aspiration experiment for measuring shear modulus

The membrane stiffness of immature reticulocytes and mature RBCs is measured through the method of micropipette aspiration in (42). Immature reticulocytes and mature RBCs from the cord blood are sorted based on the surface expression of CD71 using a magentic purification procedure. CD71 is a reliable marker for immature reticulocytes ($CD71^+$: immature reticulocytes and $CD71^-$: mature RBCs) (13,43,44). Blood smears stained with methylene blue show a reticular staining pattern, indicating the presence of residual RNA in the $CD71^+$ samples, but not in the $CD71^-$ samples (see Fig. 1, *A* and *B*). Immediately after purification, the $CD71^+$ reticulocytes are subjected to micropipette aspiration with a pipette diameter of

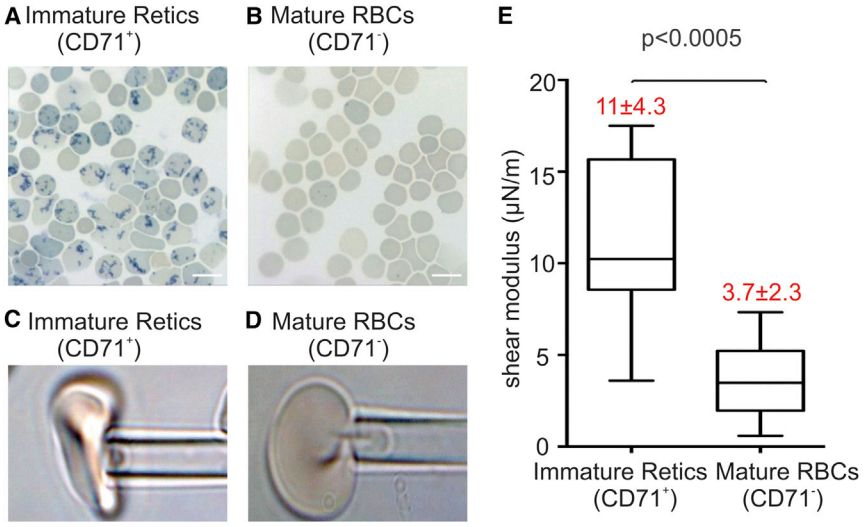

FIGURE 1 Blood smears stained with methylene blue show a reticular staining pattern indicative of residual RNA present in the $CD71^+$ population (*A*), but not in the $CD71^-$ population (*B*). Scale bars in the figures represent 10 μm. (*C*) Immature reticulocytes ($CD71^+$) and (*D*) mature RBCs ($CD71^-$) studied by using micropipette aspiration with pipette diameter 2.53 μm are shown. (*E*) The shear moduli of immature reticulocytes and mature RBCs were measured from the micropipette aspiration experiments. To see this figure in color, go online.

2.53 μm (see Fig. 1 *C*). The mature RBCs ($CD71^-$) are also measured using the same micropipette (see Fig. 1 *D*). It is noted that the morphology of reticulocytes under micropipette experiments is different from that reported in (13,45), which most likely reflects their differences in the maturation stage. As shown in Fig. 1 *E*, a remarkable decrease in shear modulus is recorded after reticulocytes mature. Precisely, a shear modulus of $\mu = 11 \pm 4.3$ μN/m is measured for the immature reticulocytes, whereas the shear modulus decreases to 3.7 ± 2.3 μN/m for mature RBCs. The larger deviation of the measurements on immature reticulocytes implies the significant heterogeneity in the maturation stage of the immature population.

Reticulocyte membrane model

In this section, we briefly review the two-component CGMD RBC membrane model and illustrate how we implement this model to construct the reticulocyte membrane model. Distinguished from the previously developed RBC membrane and RBC models (46–55), the applied membrane model represents the lipid bilayer and cytoskeleton as well as the transmembrane proteins explicitly by coarse-grained (CG) particles, allowing simulations of protein alterations or defects in the membrane of diseased RBCs (56–60). The cytoskeleton of the membrane consists of spectrin filaments connected at the actin junctional complexes, forming a hexagonal network, as shown in Fig. 2 *A*. The actin junctional complexes are represented by white particles, and they are connected to the lipid bilayer via glycophorin. Spectrin is a protein tetramer formed by head-to-head association of two identical heterodimers. Each heterodimer consists of an α-chain with 22 triple-helical segments and a β-chain with 17 triple-helical segments. Therefore, it is represented by 39 spectrin particles (*gray particles* in Fig. 2 *A*) connected by unbreakable springs. Three types of CG particles are introduced to represent the lipid bilayer of the RBC membrane. The red particles in Fig. 2, *A–D*, represent clusters of lipid molecules with a diameter of 5 nm, which is approximately equal to the thickness of the lipid bilayer. The blue particles underneath the white particles represent glycophorin proteins, and they are connected to the white particles by unbreakable springs. The green particles signify band-3 proteins, which tether spectrin filaments to the lipid bilayer. The CG particles, which form the lipid bilayer and transmembrane proteins, interact via a pairwise potential similar to the Lennard-Jones potential, except that it depends not only on translational degrees of freedom of the CG particles but also on the rotational degrees of freedom. Actin particles and spectrin filaments interact with lipid bilayer and transmembrane proteins via a Lennard-Jones potential. More details about this applied RBC membrane model and model validation can be found in the Supporting Materials and Methods. To represent the reticulocyte membrane at different stages of maturation, as shown in Fig. 2 *C*, we vary the end-to-end distance of the spectrin filaments guided by the AFM measurements reported in (15). In addition, we vary the connectivity between the action junctions and spectrin filaments in the reticulocyte membrane model, representing late synthesis of proteins 4.1 (see Fig. 2 *C*). We also vary the vertical

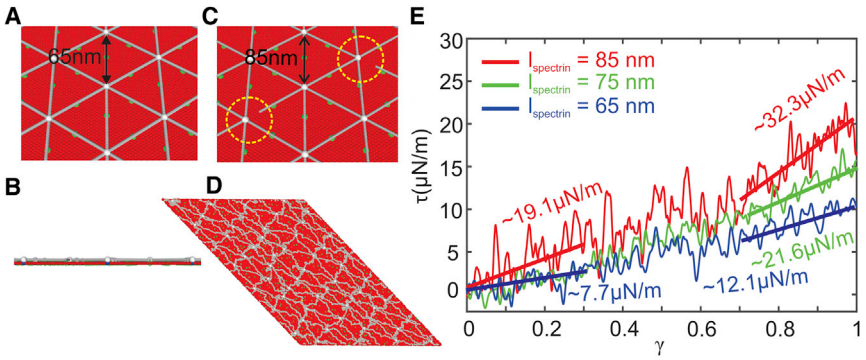

FIGURE 2 A two-component CGMD RBC membrane model, which comprises the lipid bilayer and cytoskeleton network, is applied to simulate mature RBC ((*A*): *top view* and (*B*): *side view*) and (*C*) immature reticulocyte membranes. Red particles represent lipid particles, white particles represent actin junctions, gray particles represent spectrin particles, green particles represent band-3 particles, and blue particles represent glycophorin particles. The $l_{spectrin}$ and the connectivity between the spectrin filaments and actin junctions in the reticulocyte model can be tuned to simulate reticulocytes at different stages of maturation. (*D*) The membrane is sheared to a shear strain of 1 to measure the shear modulus. (*E*) Shear stress-strain responses of the membrane for $l_{spectrin} = 65$, 75, and 85 nm, respectively, are shown. To see this figure in color, go online.

connectivity between the actin junctions and glycophorin proteins to represent the late synthesis of glycophorin C.

RESULTS AND DISCUSSION

Extended cytoskeleton enhances the reticulocyte membrane stiffness

Maturing reticulocytes become more deformable as they transition from a wrinkled globular shape to a biconcave shape (9,10). In addition to the shape effect, membrane cytoskeleton remodeling may contribute to the increased cell deformability. Considering that the surface area of reticulocytes is larger than that of erythrocytes, whereas the difference in the cytoskeletal proteins between these two groups is little (15,26), the cytoskeleton of the reticulocyte membrane could be under tension, leading to increased shear stiffness of the cell membrane. Indeed, imaging of the cytoskeleton from AFM revealed that the spectrin filaments in immature reticulocytes were elongated compared to the mature RBCs. The average $l_{spectrin}$ in the cytoskeleton of the immature reticulocyte membrane was reported to be ~17% longer than that of mature RBCs (15), which confirms our conjecture that spectrin-based meshes are extended in immature reticulocyte membranes compared to mature RBCs.

To further test our hypothesis, we build the membrane model with $l_{spectrin} = 75$ and 85 nm (see Fig. 2 *C*), which are equivalent to ~15 and ~30% increases of $l_{spectrin}$ in mature erythrocytes, representing the reticulocyte cytoskeleton at different maturation stages. The method of using proportionally varied spectrin length was successfully applied in previous modeling studies of healthy and diseased RBCs (60). Next, we evaluate the shear moduli of the membranes with varied $l_{spectrin}$ by shearing the membrane up to a shear strain of $\gamma = 1$ (see Fig. 2 *D*). The shear responses to the shear strain are illustrated in Fig. 2 *E*. When $l_{spectrin} = 65$ nm, the shear modulus of the membrane is 7.7 μN/m at small deformations, and it is increased to 12.1 μN/m at large deformations, with an average value of 9.9 μN/m. This falls within the previously reported experimental values of 4–12 μN/m (61), but it is larger than the value of 3.7 $\pm$ 2.3 μN/m measured from the micropipette experiments in this study. This difference could result from the application of 100% connectivity of cytoskeleton in the applied model, whereas the actual structure of the RBC cytoskeleton does not correspond to a perfect hexagon. We will discuss more in the following section regarding the dependence of the shear modulus on cytoskeleton connectivity. When $l_{spectrin}$ is increased to 75 nm, the average shear modulus of the membrane rises to 14.7 μN/m (*green line* in Fig. 2 *E*). At $l_{spectrin} = 85$ nm, the average shear modulus is further increased to 25.7 μN/m (*red line* in Fig. 2 *E*). Taken together, these results demonstrate that elongated spectrin filaments can elevate the shear modulus of the cell membrane, thus providing a possible explanation for the increased stiffness of reticulocytes.

Weakened cytoskeleton induces reticulocyte membrane instability

Despite increased stiffness, the membrane of reticulocytes is less stable than that of mature erythrocytes (11). This seemingly paradoxical phenomenon implies that there are different mechanisms in determining the membrane stiffness and stability (45). The stiffness of the RBC membrane arises primarily from the cytoskeleton, whereas the stability of the membrane depends on the cohesion between the cytoskeleton and the lipid bilayer as well as the integrity of the cytoskeleton. Any dissociations between the lipid bilayer and the cytoskeleton (vertical interaction) or within the cytoskeleton (horizontal interaction) cause the instability of the cell membrane, such as in blood disorders of HS (protein defects in the vertical interactions) and hereditary elliptocytosis (protein defects in the horizontal interactions) (29,62,63). Previous micropipette experiments showed that the amount of energy needed to dissociate the lipid bilayer from the cytoskeleton of immature reticulocytes was twofold smaller than that of the mature RBCs, suggesting that weakened association occurs between the cytoskeleton and lipid bilayer or within the cytoskeleton of the young reticulocytes (27). In a subsequent study, the specific protein-protein associations in the membrane of reticulocytes were examined. The results showed that whereas the spectrin proteins of immature reticulocytes are associated to the same extent as the mature RBCs, the spectrin-actin-4.1 junction complexes were vulnerable in immature reticulocytes, hence identifying the source of the membrane instability (26). This finding supports the prior speculation that the instability of the reticulocyte membrane is induced by the late synthesis and expression of protein 4.1 and glycophorin C during reticulocyte maturation (11).

In this section, we apply the reticulocyte membrane model to explore the mechanics of the reticulocyte membrane instability. To better describe the instability of reticulocytes, we construct a spherical cell based on the membrane model used in the previous section. As shown in Fig. 3 *A*, the diameter of the spherical cell is ~500 nm, and it contains 150 actin junctions. The weakened association at the spectrin-actin-4.1 junction complexes of the reticulocyte membrane is represented either by randomly reducing the connections between actin junctions and spectrin filaments, mimicking the absence of protein 4.1, or by randomly reducing the connections between the actin junctions and glycophorin proteins, mimicking the weak association of cytoskeleton to lipid bilayer. The equilibrium $l_{spectrin}$ of spectrin filaments is again selected to be 65, 75, and 85 nm, respectively.

First, we examine how the actin-spectrin connectivity (horizontal connectivity) influences the reticulocyte stability. We begin with $l_{spectrin} = 85$ nm; the horizontal connectivity ($C_{horizontal}$) is decreased from 100 to 40% at an interval of 10%, whereas the actin-glycophorin connectivity

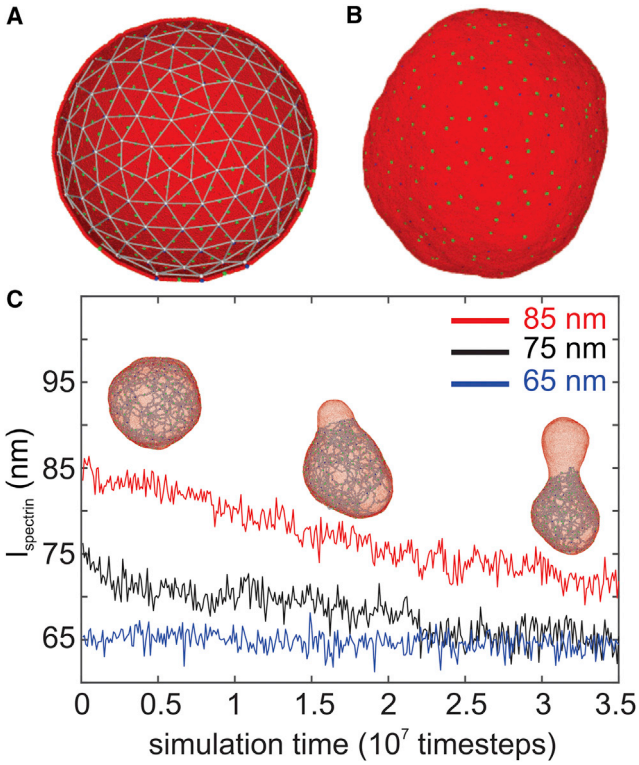

FIGURE 3 (*A*) Initial configuration of a spherical cell constructed based on the CGMD membrane model introduced in Fig. 2. It consists of 150 actin junctions with a diameter ~500 nm. (*B*) The equilibrium state of the spherical cell is shown. (*C*) $l_{spectrin}$ decreases from the initial values of 85 and 75 nm after a bud forms and grows on the spherical cell. When the initial value of $l_{spectrin}$ is 65 nm, no bud forms, and $l_{spectrin}$ remains at the initial value. To see this figure in color, go online.

is maintained at 100%. As plotted in Fig. 3 *B*, the spherical cell with $C_{horizontal} = 100\%$ maintains the spherical shape at equilibrium. Based on the measurements from the previous section, the shear modulus of the membrane with $l_{spectrin} = 85$ nm and $C_{horizontal} = 100\%$ is 25.7 μN/m, which is larger than the erythrocyte (3.7 $\pm$ 2.3 μN/m); thus, we consider that the membrane lies in a "stiff and stable" zone. When the $C_{horizontal}$ is decreased to 80%, a bud is formed at the location where the actin-spectrin connections are cut off, as shown in the insets in Fig. 3 *C*. In normal erythrocytes, the cytoskeleton is under stretch when tethered to the lipid bilayer and therefore exerts a compressive force on the lipid bilayer. This compression force is balanced by the bending resistance of the lipid bilayer (64). In the case of the reticulocyte membrane, the cytoskeleton is further extended because of the larger membrane surface area, inducing an enhanced compressive force. This compressive force is uniformly applied on the lipid bilayer when the cytoskeleton connectivity is high (e.g., $C_{horizontal} = 100$ and 90%) but becomes nonuniform as $C_{horizontal}$ is further reduced. As a result, the lipid particles are forced to migrate to the locations where the actin-spectrin connections are removed, leading to detachment of the lipid bilayer from the cytoskeleton and membrane budding (see *insets* in Fig. 3 *C*). As the bud grows, $l_{spectrin}$ reduces (see the *red curve* in Fig. 3 *C*) along with the compressive force on the lipid bilayer until it balances with the lipid bilayer bending force. The variation in the spectrin length is consistent with prior numerical (47) and analytic studies (64), which demonstrated that the spectrin length is shortened as the lipid bilayer is buckled or lost. It is noted from Fig. 2 *E* that decreased $l_{spectrin}$ leads to reduced shear modulus of the reticulocyte membrane. Considered together, our results illustrate the mechanics of membrane budding and explain the cause of the consequent decreased membrane rigidity during reticulocyte maturation.

Similar membrane-budding processes are observed for $C_{horizontal} = 80$, 70, 60, and 50% (see Fig. 4). The membrane shear moduli for these cases are obtained by shearing the membrane patches with the corresponding $l_{spectrin}$ and $C_{horizontal}$. They are computed to be 19.0, 16.4, 14.11, and 9.55 μN/m (see Fig. 5, *A* and *D*), which are larger than the shear moduli of mature erythrocytes. Hence, we consider that the membrane with the above connectivities lies in the "stiff and unstable" zone. It is noted that when $C_{horizontal} = 60$ and 50%, the average shear moduli measured from our model fall within the range of the shear modulus measured from the micropipette experiments for reticulocytes (see Fig. 5 *D*), implying that they may correspond to the cytoskeleton connectivities of the reticulocytes under the micropipette experiments. As $C_{horizontal}$ is further reduced to 40%, the elasticity of the membrane is largely compromised, and thus, the cytoskeleton cannot force the lipid bilayer to buckle. As a result, no membrane budding occurs. Fig. 5 *A* shows that when $C_{horizontal} = 40\%$, the corresponding membrane shear modulus at large shear strain is zero because of the disrupted cytoskeleton. Hence, the membrane lies in a zone of "weakened cytoskeleton," meaning that the

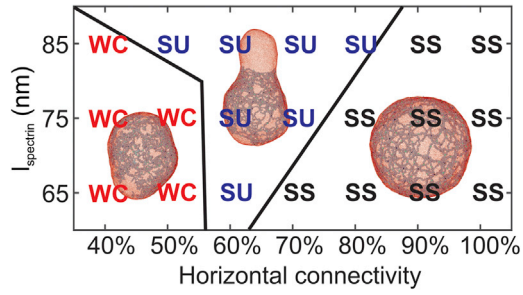

FIGURE 4 A phase diagram showing the dependence of membrane instability on the $l_{spectrin}$ and horizontal connectivity of the cytoskeleton. The vertical connectivity is maintained at 100%. SS ("stiff and stable") means that the shear modulus of the membrane is larger than that of the erythrocyte membrane, and no budding occurs. SU ("stiff and unstable") means that the shear modulus of the membrane is larger than that of the erythrocyte membrane, and membrane budding occurs. WC ("weakened cytoskeleton") means that the shear modulus of the membrane is smaller than that of the erythrocyte membrane because of low cytoskeleton connectivity, and no budding occurs. To see this figure in color, go online.

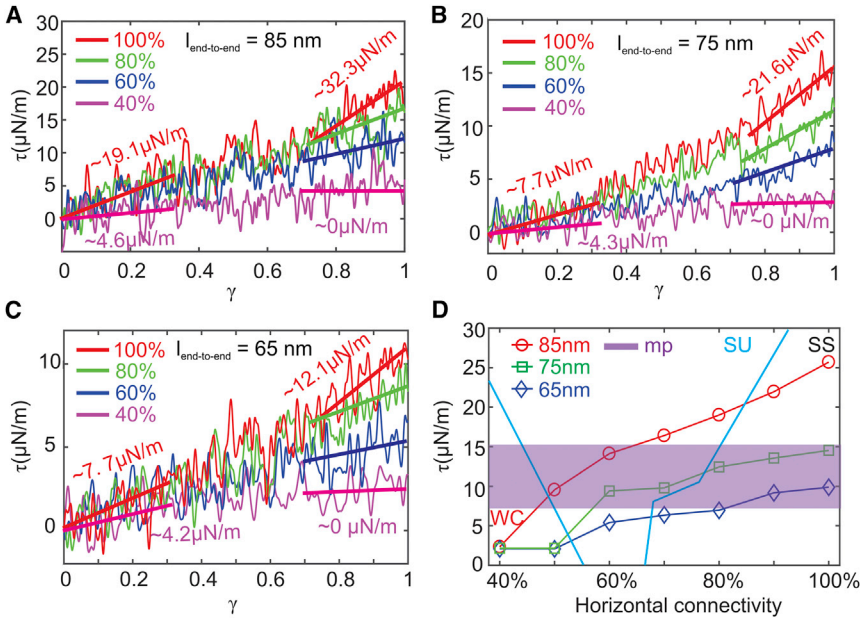

FIGURE 5 Shear stress-strain responses of the membrane at decreased connectivities of the cytoskeleton for $l_{spectrin}$ = (*A*) 85 nm, (*B*) 75 nm, and (*C*) 65 nm. (*D*) A summary of membrane shear moduli versus decreased connectivity of the cytoskeleton for $l_{spectrin}$ = 85, 75, and 65 nm, respectively, is shown. The zone with purple color highlights the values of shear moduli of immature reticulocytes measured from the micropipette experiments. The definitions of SS, SU, and WC are the same as in Fig. 4. To see this figure in color, go online.

elasticity of the membrane is damaged because of the disrupted cytoskeleton. Reticulocytes at this stage are likely to fragment or release vesicles during their passage of the narrow pathways in the microcirculation.

Subsequently, we reduce the connections between the actin junctions and glycophorin proteins to simulate the effects of phosphorylation of protein 4.1 or insufficient synthesis of glycophorin C in the reticulocyte membrane (26). The connectivity between actin junctions and glycophorin proteins is reduced from 100 to 0% at an interval of 25%. We find that the weakened association between the actin and glycophorin proteins does not change the obtained results on the instability of the spherical cell in Fig. 4. It is broadly considered that the spectrin-ankyrin-band-3 tethering sites play a dominant role in maintaining the vertical integrity of the erythrocyte membrane (29,62,65). According to a previous study on the protein-protein association in the reticulocyte membrane, the band-3 tethering sites in immature reticulocytes and mature RBCs exhibited the same level of cohesion (26), thus eliminating the possibility that weakened band-3 tethering sites induce the instability of reticulocytes. Therefore, we conclude that the weak interactions between the actin junctions and spectrin filaments mainly contribute to the membrane instability of the reticulocyte.

Next, we reduce $l_{spectrin}$ to 75 nm, and a similar transition of membrane stability from "stable and stiff" through "unstable and stiff" to "weakened cytoskeleton" is observed as $C_{horizontal}$ is decreased from 100 to 40% (see Fig. 4), except that the "unstable and stiff" zone is smaller because of less extension of the cytoskeleton. The "stiff and unstable" membrane undergoes a similar process of membrane budding, and the $l_{spectrin}$ (the *black curve* in Fig. 3 *C*) eventually approaches the $l_{spectrin}$ of erythrocytes (the *blue curve* in Fig. 3 *C*). Fig. 5 *D* shows that when $l_{spectrin} = 75$ nm, which is ~15% larger than the $l_{spectrin}$ for mature RBCs, the shear moduli measured in a wide range of $C_{horizontal}$ (from 100 to 60%) are consistent with the values of $\mu = 11 \pm 4.3$ μN/m obtained from micropipette experiments (see Fig. 1 *E*). This result cross-validates the AFM imaging of the immature reticulocyte membrane cytoskeleton, which illustrated that $l_{spectrin}$ was ~17% larger than those of mature RBCs. When $l_{spectrin} = 65$ nm, the "unstable and stiff" zone only appears at $C_{horizontal} = 60\%$, indicating that when the cytoskeleton is less stretched, such as in the mature erythrocytes, the cell membrane becomes more stable. As the $C_{horizontal}$ is reduced from 100 to 60%, the shear moduli fall from 9.9 to 5.4 μN/m, which is comparable with the value of 3.7 $\pm$ 2.3 μN/m measured from micropipette experiments. When $C_{horizontal} = 50$ and 40%, the cytoskeleton becomes disrupted at large shear strain, and membrane falls into the "weakened cytoskeleton" zone, as illustrated in Fig. 4.

Considered together, our simulations elucidate the process of stiffness and stability changes during reticulocyte maturation. Also, we conclude that the extended cytoskeleton network in the reticulocytes along with the weakened actin junction complexes contributes to the seemingly paradoxical phenomenon that the reticulocytes are stiffer but less stable than the mature erythrocytes. It is noted that all the above simulations are performed without considering the environmental effects, such as cells passing through capillaries or the interendothelial slits in the spleen, where they may undergo drastic deformations. In our simulations, the detachment of the lipid bilayer is caused by the interaction between the lipid bilayer and cytoskeleton alone. External disturbances definitely could exacerbate the instability of the cell membrane and induce more pronounced membrane

budding and vesiculation. For example, although RBCs with membranes in the "weakened cytoskeleton" zone do not bud spontaneously, they are more likely to shed vesicles or rupture when under significant external stress because of the compromised cell elasticity.

Membrane budding, a second mechanism of shedding plasma membrane

Recently, membrane budding was proposed as a second mechanism of shedding plasma membrane after reticulocytes are released to peripheral circulation (16). Examination of the released vesicles revealed the presence of glycophorin A and other integral membrane proteins, such as band-3 and GLUT 1, and the absence of the cytoskeletal proteins, like spectrin, ankyrin, and actin. This finding implies that these released vesicles were derived from regions where the lipid bilayer was not supported by the cytoskeleton (16). However, it is not clear whether this membrane budding is part of the continuous process of exocytosis or whether it occurs independently because of the instability of the reticulocytes. Our simulations show that membrane budding can be induced by the weakened association at the spectrin-actin-4.1 junction complexes, thereby demonstrating that membrane budding can be an independent process for reticulocytes. In particular, the membrane budding is initiated from the region where the cytoskeleton is disrupted, confirming the hypothesis that the vesicles released from reticulocytes were derived from the membrane surface area that is free of cytoskeleton (16). However, it does not exclude the possibility that the membrane-budding regions originated from fusing the cell membrane with multivesicular bodies, as a final step of the exocytosis process. Either way, shedding membrane from the region where the cohesion between lipid bilayer and cytoskeleton is low could serve as a means of removing the redundant surface area from reticulocytes, thereby optimizing the interaction between the lipid bilayer and cytoskeleton (16).

HS RBCs begin shedding membrane at the reticulocyte stage

In HS, defects occur in the RBC membrane proteins that account for the vertical linkages between the cytoskeleton and the lipid bilayer, such as ankyrin, protein 4.2, band-3, and spectrin (29,62,66). These protein defects weaken the vertical cohesion between the cytoskeleton and the lipid bilayer in RBCs, causing surface area loss through releasing vesicles. HS RBCs with reduced surface area transform progressively from a biconcave shape to a near-spherical shape. The spherical RBCs are less deformable and thus are removed by the spleen prematurely. It is broadly considered that HS RBCs shed surface area predominantly during their sojourn in circulation. However, a prior experimental study discovered that loss of surface area by HS RBCs begins at the reticulocyte stage (10), contradicting the prevailing hypothesis. Here, we introduce defective band-3 proteins into the spherical cell model by breaking the connections between band-3 particles and spectrin filaments (vertical connectivity), and we examine how the weakened spectrin-ankyrin-band-3 tethering sites affect the membrane stability. We reduce the vertical connectivity (C_{vertical}) from 100 to 0% at an interval of 25% while $C_{\text{horizontal}}$ is maintained at 100% to examine the effect of vertical interactions on membrane stability exclusively. At $l_{\text{spectrin}} = 85$ nm, lipid bilayer detachment and membrane budding are observed when C_{vertical} is decreased to 50% (see Fig. 6), indicating that reducing the vertical connection can aggravate the membrane instability. As l_{spectrin} is reduced to 75 nm, membrane budding only occurs when $C_{\text{vertical}} = 0\%$ (see Fig. 6). In the case of $l_{\text{spectrin}} = 65$ nm, the cell membrane remains stable for all values of C_{vertical}. The above simulations illustrate that reducing the cohesion between the cytoskeleton and the lipid bilayer, such as in HS, promotes the membrane budding and therefore the consequent vesiculation from the reticulocyte membrane ($l_{\text{spectrin}} = 75$ and 85 nm). These results indicate that reticulocytes are more likely to form buds than mature erythrocytes when the vertical cohesion of the membrane is weak, thereby explaining the previous experimental finding that HS RBCs started shedding membrane more aggressively at the reticulocyte stage (10). Again, we would like to emphasize that the budding of the lipid bilayer in this simulation is induced by the interactions between lipid bilayer and cytoskeleton only. When $l_{\text{spectrin}} = 75$ nm and C_{vertical} is low, although detachment between the lipid bilayer and cytoskeleton was not observed from our simulations, it is likely to be stimulated when HS reticulocytes are under external stresses or disturbances.

CONCLUSIONS

In this work, we develop a CGMD reticulocyte membrane model to investigate how the structural changes in

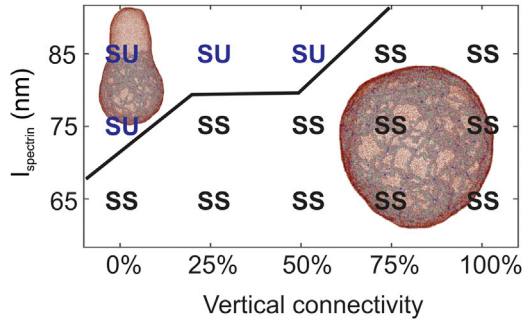

FIGURE 6 A phase diagram showing the dependence of membrane instability on the l_{spectrin} and the vertical connectivity between band-3 protein and spectrin filaments. The horizontal connectivity is maintained at 100%. The definitions of SS and SU are the same as in Fig. 4. To see this figure in color, go online.

cytoskeleton alter the stiffness and stability of reticulocytes. Our simulation results demonstrate that the extended cytoskeleton network in the reticulocytes along with the weakened association at actin junction complexes contributes to the experimental finding that reticulocytes are stiffer but less stable than mature erythrocytes. We also find that budding of the reticulocyte membrane can be induced by reducing the cytoskeleton connectivity, which confirms a previous hypothesis that membrane budding can occur independently in reticulocytes and thus serve as a second mechanism of shedding plasma membrane as reticulocytes mature. Earlier in the manuscript, we demonstrated that the weakened cohesion between the lipid bilayer and the cytoskeleton promotes membrane budding in HS, which explains why the HS RBCs may lose surface membrane at the reticulocyte stage.

Our studies on the reticulocyte membrane also shed light on understanding why *P. vivax* and *P. falciparum* prefer invading young reticulocytes from a biomechanical perspective. The infection of RBCs by malaria has been a topic of extensive research, but the cell age preference of the parasites is assumed to predominantly rely on the presence of particular ligands at the apical ends of the invasive merozoites and the corresponding receptors on the host cell membrane (67–69). The role of the particular biomechanical properties of reticulocytes in the malaria invasion has never been considered. Merozoites invade erythrocytes by inducing rapid and localized membrane invagination, followed by tight junction formation, fusion of the rhoptries with the erythrocyte membrane, and final fission to close the erythrocyte and vacuolar membranes (70). As the function of the cytoskeleton is to maintain the integrity of membrane, an intact and dense cytoskeleton is likely to work as a more effective physical barrier to prohibit the merozoite invasion. However, the weakened association at the actin junction complexes in the reticulocyte membrane can compromise the resistance of the membrane to the parasites. In addition, the instability of the reticulocytes could facilitate the membrane invagination. Therefore, we hypothesize that the two characteristics of the reticulocyte membrane that we discovered in this work (extended cytoskeleton and reduced cytoskeleton connectivity) are at least partially ascribed to the fact that *P. vivax* and *P. falciparum* favor reticulocytes for invasion.

To the best of our knowledge, the CGMD reticulocyte membrane model that we present here is the first of its kind. It is developed on the basis of the currently available experimental data on the cytoskeleton structure of reticulocytes as well as the protein expression and association in the reticulocyte membrane (15,26). However, this model is constructed under several assumptions, and hence, it has limitations. For example, the AFM imaging showed that the average $l_{spectrin}$ in the cytoskeletons of immature and mature erythrocyte membranes were ~41 and ~48 nm (15), respectively. These values are substantially shorter than the consensus values of 65–70 nm that we used to construct our model (71–75). This discrepancy may arise from particular techniques applied in AFM imaging (76,77), but overall, the AFM measurements confirm our conjecture that a spectrin-based network is extended in immature reticulocyte membranes. Thus, we increased $l_{spectrin}$ in our model proportionally following the data reported in the AFM measurements to represent the reticulocytes at different maturation stages. Moreover, in our model, we did not consider the metabolic activity that could contribute to the dynamic remodeling of the reticulocyte cytoskeleton, which, in turn, could play a role in determining the biomechanical properties of reticulocytes during their maturation. Our results on the instability of reticulocytes and membrane budding, presented collectively as the phase diagrams in Figs. 4 and 6, are based on the aforementioned assumptions and analysis of the mechanics of the lipid bilayer and cytoskeleton. Therefore, our findings require further experimental cross-validation and refinement, and we hope that these simulation-based phase diagrams can potentially stimulate and steer new experiments in this area. Multimodality data from future experiments also can be used to further improve our model.

SUPPORTING MATERIAL

Supporting Materials and Methods are available at http://www.biophysj.org/biophysj/supplemental/S0006-3495(18)30321-7.

AUTHOR CONTRIBUTIONS

H.L., J.Y., T.T.C., R.C., M.D., and G.E.K. designed the research. H.L., J.Y., R.N., and T.T.C. performed the research. H.L., J.Y., T.T.C., R.N., and L.L. analyzed the data. H.L., J.Y., T.T.C., R.C., M.D., and G.E.K. wrote the article.

ACKNOWLEDGMENTS

The work described in this article was supported by National Institutes of Health grant numbers U01HL114476 and U01HL116323. An award of computer time was provided by the Innovative and Novel Computational Impact on Theory and Experiment program. This research used resources from the Argonne Leadership Computing Facility, which is supported by the Department of Energy Office of Science User Facility under contract number DE-AC02-06CH11357. This research also used resources from the Oak Ridge Leadership Computing Facility, which is supported by the Department of Energy Office of Science User Facility under contract number DE-AC05-00OR22725. T.T.C. and M.D. acknowledge support from the Singapore-MIT Alliance for Research and Technology. J.Y. and M.D. acknowledge partial support from National Institutes of Health grant number 1R01HL121386-01A1. R.C. acknowledges funding received from the Singapore University of Technology & Design through the Ministry of Education Tier 1 grant (T1MOE1702).

REFERENCES

1. Manwani, D., and J. J. Bieker. 2008. The erythroblastic island. *Curr. Top. Dev. Biol.* 82:23–53.

2. An, X., and N. Mohandas. 2011. Erythroblastic islands, terminal erythroid differentiation and reticulocyte maturation. *Int. J. Hematol.* 93:139–143.
3. Griffiths, R. E., S. Kupzig, …, J. D. Lane. 2012. The ins and outs of human reticulocyte maturation: autophagy and the endosome/exosome pathway. *Autophagy.* 8:1150–1151.
4. Harding, C., J. Heuser, and P. Stahl. 1983. Receptor-mediated endocytosis of transferrin and recycling of the transferrin receptor in rat reticulocytes. *J. Cell Biol.* 97:329–339.
5. Pan, B. T., K. Teng, …, R. M. Johnstone. 1985. Electron microscopic evidence for externalization of the transferrin receptor in vesicular form in sheep reticulocytes. *J. Cell Biol.* 101:942–948.
6. Johnstone, R. M., M. Adam, …, C. Turbide. 1987. Vesicle formation during reticulocyte maturation. Association of plasma membrane activities with released vesicles (exosomes). *J. Biol. Chem.* 262:9412–9420.
7. Blanc, L., A. De Gassart, …, M. Vidal. 2005. Exosome release by reticulocytes–an integral part of the red blood cell differentiation system. *Blood Cells Mol. Dis.* 35:21–26.
8. Lew, V. L., J. E. Raftos, …, N. Mohandas. 1995. Generation of normal human red cell volume, hemoglobin content, and membrane area distributions by "birth" or regulation? *Blood.* 86:334–341.
9. Waugh, R. E., J. B. McKenney, …, L. M. Snyder. 1997. Surface area and volume changes during maturation of reticulocytes in the circulation of the baboon. *J. Lab. Clin. Med.* 129:527–535.
10. Da Costa, L., N. Mohandas, …, T. Cynober. 2001. Temporal differences in membrane loss lead to distinct reticulocyte features in hereditary spherocytosis and in immune hemolytic anemia. *Blood.* 98:2894–2899.
11. Chasis, J. A., M. Prenant, …, N. Mohandas. 1989. Membrane assembly and remodeling during reticulocyte maturation. *Blood.* 74:1112–1120.
12. Waugh, R. E. 1991. Reticulocyte rigidity and passage through endothelial-like pores. *Blood.* 78:3037–3042.
13. Malleret, B., F. Xu, …, B. Russell. 2013. Significant biochemical, biophysical and metabolic diversity in circulating human cord blood reticulocytes. *PLoS One.* 8:e76062.
14. Mel, H. C., M. Prenant, and N. Mohandas. 1977. Reticulocyte motility and form: studies on maturation and classification. *Blood.* 49:1001–1009.
15. Chu, T. T. T., A. Sinha, …, R. Chandramohanadas. 2018. Quantitative mass spectrometry of human reticulocytes reveal proteome-wide modifications during maturation. *Br. J. Haematol.* 180:118–133.
16. Griffiths, R. E., S. Kupzig, …, D. J. Anstee. 2012. Maturing reticulocytes internalize plasma membrane in glycophorin A-containing vesicles that fuse with autophagosomes before exocytosis. *Blood.* 119:6296–6306.
17. Malleret, B., A. Li, …, B. Russell. 2015. Plasmodium vivax: restricted tropism and rapid remodeling of CD71-positive reticulocytes. *Blood.* 125:1314–1324.
18. Chasis, J. A., and S. L. Schrier. 1989. Membrane deformability and the capacity for shape change in the erythrocyte. *Blood.* 74:2562–2568.
19. Chang, H., P. J. Langer, and H. F. Lodish. 1976. Asynchronous synthesis of erythrocyte membrane proteins. *Proc. Natl. Acad. Sci. USA.* 73:3206–3210.
20. Krasnow, S. H., H. J. Pielichowski, …, S. K. Ballas. 1981. Membrane proteins synthesized by human reticulocytes and their precursors. *Br. J. Haematol.* 47:171–183.
21. Blikstad, I., W. J. Nelson, …, E. Lazarides. 1983. Synthesis and assembly of spectrin during avian erythropoiesis: stoichiometric assembly but unequal synthesis of α and β spectrin. *Cell.* 32:1081–1091.
22. Staufenbiel, M., and E. Lazarides. 1986. Assembly of protein 4.1 during chicken erythroid differentiation. *J. Cell Biol.* 102:1157–1163.
23. Hanspal, M., and J. Palek. 1987. Synthesis and assembly of membrane skeletal proteins in mammalian red cell precursors. *J. Cell Biol.* 105:1417–1424.
24. Boal, D. 2012. Mechanics of the Cell. Cambridge University Press, Cambridge, UK.
25. Ohanian, V., L. C. Wolfe, …, W. B. Gratzer. 1984. Analysis of the ternary interaction of the red cell membrane skeletal proteins spectrin, actin, and 4.1. *Biochemistry.* 23:4416–4420.
26. Liu, J., X. Guo, …, X. An. 2010. Membrane remodeling during reticulocyte maturation. *Blood.* 115:2021–2027.
27. Waugh, R. E., Y. S. Huang, …, J. Palis. 2013. Development of membrane mechanical function during terminal stages of primitive erythropoiesis in mice. *Exp. Hematol.* 41:398–408.e2.
28. Goldberg, M. A., C. Brugnara, …, H. F. Bunn. 1990. Treatment of sickle cell anemia with hydroxyurea and erythropoietin. *N. Engl. J. Med.* 323:366–372.
29. Da Costa, L., J. Galimand, …, N. Mohandas. 2013. Hereditary spherocytosis, elliptocytosis, and other red cell membrane disorders. *Blood Rev.* 27:167–178.
30. Kaul, D. K., M. E. Fabry, …, R. L. Nagel. 1983. Erythrocytes in sickle cell anemia are heterogeneous in their rheological and hemodynamic characteristics. *J. Clin. Invest.* 72:22–31.
31. Mohandas, N., and E. Evans. 1985. Sickle erythrocyte adherence to vascular endothelium. Morphologic correlates and the requirement for divalent cations and collagen-binding plasma proteins. *J. Clin. Invest.* 76:1605–1612.
32. Kaul, D. K., D. Chen, and J. Zhan. 1994. Adhesion of sickle cells to vascular endothelium is critically dependent on changes in density and shape of the cells. *Blood.* 83:3006–3017.
33. Pasvol, G., D. J. Weatherall, and R. J. Wilson. 1980. The increased susceptibility of young red cells to invasion by the malarial parasite Plasmodium falciparum. *Br. J. Haematol.* 45:285–295.
34. Mons, B. 1990. Preferential invasion of malarial merozoites into young red blood cells. *Blood Cells.* 16:299–312.
35. Triglia, T., J. Thompson, …, A. F. Cowman. 2001. Identification of proteins from Plasmodium falciparum that are homologous to reticulocyte binding proteins in Plasmodium vivax. *Infect. Immun.* 69:1084–1092.
36. McKenzie, F. E., G. M. Jeffery, and W. E. Collins. 2002. Plasmodium vivax blood-stage dynamics. *J. Parasitol.* 88:521–535.
37. Duraisingh, M. T., T. Triglia, …, A. F. Cowman. 2003. Phenotypic variation of Plasmodium falciparum merozoite proteins directs receptor targeting for invasion of human erythrocytes. *EMBO J.* 22:1047–1057.
38. Stubbs, J., K. M. Simpson, …, A. F. Cowman. 2005. Molecular mechanism for switching of P. falciparum invasion pathways into human erythrocytes. *Science.* 309:1384–1387.
39. Zweig, S. E., K. T. Tokuyasu, and S. J. Singer. 1981. Member-associated changes during erythropoiesis. On the mechanism of maturation of reticulocytes to erythrocytes. *J. Supramol. Struct. Cell. Biochem.* 17:163–181.
40. Blanc, L., and M. Vidal. 2010. Reticulocyte membrane remodeling: contribution of the exosome pathway. *Curr. Opin. Hematol.* 17:177–183.
41. Ney, P. A. 2011. Normal and disordered reticulocyte maturation. *Curr. Opin. Hematol.* 18:152–157.
42. Sinha, A., T. T. Chu, …, R. Chandramohanadas. 2015. Single-cell evaluation of red blood cell bio-mechanical and nano-structural alterations upon chemically induced oxidative stress. *Sci. Rep.* 5:9768.
43. Brun, A., G. Gaudernack, and S. Sandberg. 1990. A new method for isolation of reticulocytes: positive selection of human reticulocytes by immunomagnetic separation. *Blood.* 76:2397–2403.
44. Kono, M., T. Kondo, …, K. Fujimoto. 2009. Morphological definition of CD71 positive reticulocytes by various staining techniques and electron microscopy compared to reticulocytes detected by an automated hematology analyzer. *Clin. Chim. Acta.* 404:105–110.
45. Chasis, J. A., and N. Mohandas. 1986. Erythrocyte membrane deformability and stability: two distinct membrane properties that are independently regulated by skeletal protein associations. *J. Cell Biol.* 103:343–350.

46. Drouffe, J. M., A. C. Maggs, and S. Leibler. 1991. Computer simulations of self-assembled membranes. *Science.* 254:1353–1356.

47. Discher, D. E., D. H. Boal, and S. K. Boey. 1998. Simulations of the erythrocyte cytoskeleton at large deformation. II. Micropipette aspiration. *Biophys. J.* 75:1584–1597.

48. Goetz, R., G. Gompper, and R. Lipowsky. 1999. Mobility and elasticity of self-assembled membranes. *Phys. Rev. Lett.* 82:221.

49. Li, J., M. Dao, …, S. Suresh. 2005. Spectrin-level modeling of the cytoskeleton and optical tweezers stretching of the erythrocyte. *Biophys. J.* 88:3707–3719.

50. Cooke, I. R., K. Kremer, and M. Deserno. 2005. Tunable generic model for fluid bilayer membranes. *Phys. Rev. E Stat. Nonlin. Soft Matter Phys.* 72:011506.

51. Pivkin, I. V., and G. E. Karniadakis. 2008. Accurate coarse-grained modeling of red blood cells. *Phys. Rev. Lett.* 101:118105.

52. Yuan, H., C. Huang, …, S. Zhang. 2010. One-particle-thick, solvent-free, coarse-grained model for biological and biomimetic fluid membranes. *Phys. Rev. E Stat. Nonlin. Soft Matter Phys.* 82:011905.

53. Li, H., and G. Lykotrafitis. 2012. Two-component coarse-grained molecular-dynamics model for the human erythrocyte membrane. *Biophys. J.* 102:75–84.

54. Peng, Z., X. Li, …, S. Suresh. 2013. Lipid bilayer and cytoskeletal interactions in a red blood cell. *Proc. Natl. Acad. Sci. USA.* 110:13356–13361.

55. Li, H., H. Chang, …, G. Lykotrafitis. 2018. Modeling biomembranes and red blood cells by coarse-grained particle methods. *Appl. Math. Mech.* 39:3–20.

56. Li, H., and G. Lykotrafitis. 2015. Vesiculation of healthy and defective red blood cells. *Phys. Rev. E Stat. Nonlin. Soft Matter Phys.* 92:012715.

57. Li, H., Y. Zhang, …, G. Lykotrafitis. 2016. Modeling of band-3 protein diffusion in the normal and defective red blood cell membrane. *Soft Matter.* 12:3643–3653.

58. Zhang, Y., C. Huang, …, S. Suresh. 2015. Multiple stiffening effects of nanoscale knobs on human red blood cells infected with Plasmodium falciparum malaria parasite. *Proc. Natl. Acad. Sci. USA.* 112:6068–6073.

59. Chang, H. Y., X. Li, …, G. E. Karniadakis. 2016. MD/DPD multiscale framework for predicting morphology and stresses of red blood cells in health and disease. *PLoS Comput. Biol.* 12:e1005173.

60. Dearnley, M., T. Chu, …, L. Tilley. 2016. Reversible host cell remodeling underpins deformability changes in malaria parasite sexual blood stages. *Proc. Natl. Acad. Sci. USA.* 113:4800–4805.

61. Hochmuth, R. M., and R. E. Waugh. 1987. Erythrocyte membrane elasticity and viscosity. *Annu. Rev. Physiol.* 49:209–219.

62. An, X., and N. Mohandas. 2008. Disorders of red cell membrane. *Br. J. Haematol.* 141:367–375.

63. Mohandas, N., and P. G. Gallagher. 2008. Red cell membrane: past, present, and future. *Blood.* 112:3939–3948.

64. Sens, P., and N. Gov. 2007. Force balance and membrane shedding at the red-blood-cell surface. *Phys. Rev. Lett.* 98:018102.

65. Gov, N. S. 2007. Less is more: removing membrane attachments stiffens the RBC cytoskeleton. *New J. Phys.* 9:429.

66. Li, X., H. Li, …, G. E. Karniadakis. 2017. Computational biomechanics of human red blood cells in hematological disorders. *J. Biomech. Eng.* 139:021008.

67. Cowman, A. F., and B. S. Crabb. 2006. Invasion of red blood cells by malaria parasites. *Cell.* 124:755–766.

68. Mohandas, N., and X. An. 2012. Malaria and human red blood cells. *Med. Microbiol. Immunol.* 201:593–598.

69. Paul, A. S., E. S. Egan, and M. T. Duraisingh. 2015. Host-parasite interactions that guide red blood cell invasion by malaria parasites. *Curr. Opin. Hematol.* 22:220–226.

70. Zuccala, E. S., and J. Baum. 2011. Cytoskeletal and membrane remodelling during malaria parasite invasion of the human erythrocyte. *Br. J. Haematol.* 154:680–689.

71. Steck, T. L. 1974. The organization of proteins in the human red blood cell membrane. A review. *J. Cell Biol.* 62:1–19.

72. Evans, E. A., and P. L. La Celle. 1975. Intrinsic material properties of the erythrocyte membrane indicated by mechanical analysis of deformation. *Blood.* 45:29–43.

73. Shen, B. W., R. Josephs, and T. L. Steck. 1986. Ultrastructure of the intact skeleton of the human erythrocyte membrane. *J. Cell Biol.* 102:997–1006.

74. Vertessy, B. G., and T. L. Steck. 1989. Elasticity of the human red cell membrane skeleton. Effects of temperature and denaturants. *Biophys. J.* 55:255–262.

75. Lux, S. E., IV 2016. Anatomy of the red cell membrane skeleton: unanswered questions. *Blood.* 127:187–199.

76. Takeuchi, M., H. Miyamoto, …, A. Kusumi. 1998. Structure of the erythrocyte membrane skeleton as observed by atomic force microscopy. *Biophys. J.* 74:2171–2183.

77. Swihart, A. H., J. M. Mikrut, …, R. C. Macdonald. 2001. Atomic force microscopy of the erythrocyte membrane skeleton. *J. Microsc.* 204:212–225.

Biophysical Journal, Volume *114*

Supplemental Information

Cytoskeleton Remodeling Induces Membrane Stiffness and Stability Changes of Maturing Reticulocytes

He Li, Jun Yang, Trang T. Chu, Renugah Naidu, Lu Lu, Rajesh Chandramohanadas, Ming Dao, and George Em Karniadakis

The RBC membrane model and validation

The applied coarse-grained molecular dynamics (CGMD) membrane model describes the RBC membrane as a two-component system, including the cytoskeleton and the lipid bilayer. The lipid bilayer is represented by three types of CG particles, including lipid particles, band-3 particles and glycophrin particles. The cytoskeleton consists of two types of CG particles, representing action junction complex and spectrin proteins. The cytoskeleton consists of the hexagonal spectrin network and actin junctions. The actin junctions are connected to the lipid bilayer via glycophorin. As shown in Fig. 2(A-B), the spectrin filament is represented by 39 spectrin particles (grey particles) connected by unbreakable springs. The spring potential, $u_{\mathbf{cy}}^{\mathbf{s\text{-}s}}(r) = k_0(r - r_{\mathbf{eq}}^{\mathbf{s\text{-}s}})^2/2$, with equilibrium distance $r_{\mathbf{eq}}^{\mathbf{s\text{-}s}} = L_{\max}/39$, where $L_{\max}$ is the contour length of the spectrin (~200 nm) and $r_{\mathbf{eq}}^{\mathbf{s\text{-}s}} \cong 5\,\text{nm}$. The spectrin chain is connected to the band-3 particles (white particles). The two ends of the spectrin chains are connected to the actin junction via a spring potential, $u_{\mathbf{cy}}^{\mathbf{a\text{-}s}}(r) = k_0(r - r_{\mathbf{eq}}^{\mathbf{a\text{-}s}})^2/2$ where the equilibrium distance $r_{\mathbf{eq}}^{\mathbf{a\text{-}s}} = 10\,\text{nm}$. The spring constant is determined subsequently. The spectrin particles, which are not connected by the spring potential, interact with each other via the repulsive part of the L-J potential

$$u_{rep}(r_{ij}) = \begin{cases} 4\varepsilon\left[\left(\frac{\sigma}{r_{ij}}\right)^{12} - \left(\frac{\sigma}{r_{ij}}\right)^{6}\right] & r_{ij} < R_{cut,LJ} \\ 0 & r_{ij} \geq R_{cut,LJ} \end{cases} \quad (1)$$

where ε is the energy unit and σ is the length unit. r_{ij} is the distance between the spectrin particles. The cutoff distance of the potential $R_{\text{cut,LJ}}$ is chosen to the equilibrium distances $r_{\mathbf{eq}}^{\mathbf{s\text{-}s}}$ between the spectrin particles. The spring constant k_0 is selected to be $1000\varepsilon/\sigma^2$.

The CG particles, which form the lipid bilayer and transmembrane proteins, carry both translational and rotational degrees of freedom ($\mathbf{x}_i$, $\mathbf{n}_i$), where $\mathbf{x}_i$ and $\mathbf{n}_i$ are the position and the orientation (direction vector) of particle *i*, respectively. The rotational degrees of freedom obey the normality condition $|\mathbf{n}_i| = 1$. Thus, each CG particle effectively carries 5 degrees of freedom. $\mathbf{x}_{ij} = \mathbf{x}_j - \mathbf{x}_i$ is defined as the distance vector between particles *i* and *j*. Correspondingly, $r_{ij} \equiv |\mathbf{x}_{ij}|$ is the distance, and $\hat{\mathbf{x}}_{\mathbf{ij}} = \mathbf{x}_{\mathbf{ij}}/r_{\mathbf{ij}}$ is a unit vector. The CG particles, forming the lipid membrane and membrane proteins, interact with one another via a pair-wise additive potential

$$u_{\text{mem}}(\mathrm{n}_i, \mathrm{n}_j, \mathrm{x}_{ij}) = u_{\mathrm{R}}(r_{ij}) + A\left(\alpha, a(\mathrm{n}_i, \mathrm{n}_j, \mathrm{x}_{ij})\right) u_{\mathrm{A}}(r_{ij}), \quad (2)$$

$$\begin{cases} u_R(r_{ij}) = k\varepsilon\left(\left(R_{cut,mem} - r_{ij}\right)/\left(R_{cut,mem} - r_{eq}\right)\right)^8 - k\varepsilon & \text{for} \quad r_{ij} < R_{cut,mem} \\ u_A(r_{ij}) = -2k\varepsilon\left(\left(R_{cut,mem} - r_{ij}\right)/\left(R_{cut,mem} - r_{eq}\right)\right)^4 - k\varepsilon & \text{for} \quad r_{ij} < R_{cut,mem} \\ u_R(r_{ij}) = u_A(r_{ij}) = 0, & \text{for} \quad r_{ij} \geq R_{cut,mem} \end{cases} \quad (3)$$

where $u_R(r_{ij})$ and $u_A(r_{ij})$ are the repulsive and attractive components of the pair potential, respectively. α is a tunable linear amplification factor. The function $A(\alpha,a(\mathbf{n}_i,\mathbf{n}_j,\mathbf{x}_{ij}))= 1+\alpha(a(\mathbf{n}_i,\mathbf{n}_j,\mathbf{x}_{ij}) -1)$ tunes the energy well of the potential. In the simulations, α is chosen to be 1.55 and cutoff distance of the potential $R_{cut,mem}$ is chosen to be 2.6σ. The detailed information about applied potentials and the selection of the potential parameters can be found from author's previous work (1). k is selected to be 1.2 for the interactions among the lipid particles and k = 2.8 for interactions between the lipid and the protein particles, such as glycophorin and band-3. Given the diameter of the lipid particles $r_{lipid} = 2^{1/6}\sigma$ = 5 nm, the length unit is calculated to be σ = 4.45 nm. The temperature of the system is maintained at k_BT/ε = 0.22 by employing the Nose-Hoover thermostat. At equilibrium, the average end-to-end spectrin length is ~65 nm.

The key mechanical property of erythrocyte membrane is the shear modulus. In order to compute the shear modulus of the RBC membrane, we shear the membrane to a shear strain (γ) of 1, as shown in Fig. 2D. Based on the shear response of the RBC membrane, we found the shear modulus of the membrane is ~7.7 μN/m at small deformation while it is increased to ~12.1 μN/m at large deformation, which is consistent with the experimentally measured values of 4–12 μN/m (2).

References

1. Li, H., and G. Lykotrafitis. 2014. Erythrocyte membrane model with explicit description of the lipid bilayer and the spectrin network. *Biophysical Journal* 107:642-653.
2. Hochmuth, R., and R. Waugh. 1987. Erythrocyte membrane elasticity and viscosity. *Annual Review of Physiology* 49:209-219.